Marangoni instability in a liquid layer bounded by two coaxial cylinder surfaces

Hoefsloot, H.C.J.; Hoogstraten, H.W.; Hoven, A.; Janssen, L.P.B.M.

Published in:
Applied Scientific Research

DOI:
10.1007/BF00386464

Applied Scientific Research **47**: 1–21, 1990.

Marangoni instability in a liquid layer bounded by two coaxial cylinder surfaces

H.C.J. HOEFSLOOT*, H.W. HOOGSTRATEN‡, A. HOVEN‡ & L.P.B.M. JANSSEN*

Departments of Chemical Engineering and Mathematics‡, University of Groningen, Groningen, The Netherlands*

Received 27 December 1988; accepted in revised form 2 July 1989

Abstract. A liquid layer, confined between two coaxial cylinder surfaces, has either a gas–liquid interface on the inside and is heated from the outer (solid) boundary, or it has a gas–liquid interface on the outside and is heated from the inner (solid) boundary. Neglecting gravity and using a standard normal-mode approach, we analyse surface-tension driven instability (Marangoni instability) of the motionless steady state in which the temperature depends on the radial coordinate only. Numerical results for the critical Marangoni number and corresponding wave-number pair are presented for various values of the curvature of the interface. This curvature turns out to exert a significant influence on the onset of Marangoni convection flows. Further, the stability behaviour of the system is found to be quite variable, depending on whether the interface is on the inside or on the outside of the layer and whether it is well-conducting or nearly-isolated.

1. Introduction

When a quiescent liquid layer is heated from below cellular convection flow patterns consisting of so-called roll cells (or Bénard cells) can be observed to develop under certain circumstances. Similar phenomena may occur in liquids containing a solute that can evaporate at a gas–liquid interface. Two different mechanisms are commonly considered to be responsible for this type of instability: (*i*) buoyancy effects caused by density variations (Rayleigh convection) and (*ii*) surface tractions caused by surface-tension variations that may arise from the surface tension's dependence on the temperature or solute concentration (Marangoni convection). Cellular convection was first intensively studied by Bénard in 1900, and an explanation as its being the result of buoyancy effects has first been given in 1916 by Lord Rayleigh. Much later Pearson [5], neglecting gravity, presented an explanation based on surface-tension arguments. The coupling between the two agencies was studied by Nield [4].

One of Nield's conclusions was that for thin liquid layers surface-tension effects will be more important than buoyancy. This dominance of Marangoni

convection is of particular interest in chemical engineering equipment where thin liquid films occur frequently in, for example, the flow of a gas–liquid mixture in a packed-bed column. The presence of roll-cell activity in such a column is considered to be favourable, since it enhances heat and/or mass transfer between the two phases, thus leading to an improvement of the column's efficiency. Contrary to the cases treated by Pearson, Nield and others, who considered only planar gas–liquid interfaces, the liquid films occurring in packed-bed columns will mostly have curved interfaces.

Unfortunately experimental work on Marangoni convection in thin liquid layers is seriously hampered by the difficulty of performing flow measurements in such layers. For that reason, a series of experiments under microgravity conditions has been performed under the auspices of the Chemical Engineering Department of the University of Groningen, the Netherlands [1, 3]. Because of microgravity buoyancy is inoperative, so surface-tension effects alone will be responsible for roll-cell formation, even in deep liquid layers. In the experiments it was possible to study the creation of Marangoni convection flows (*i*) in a liquid layer consisting of an acetone solution in water bounded above by either a planar or a curved gas–liquid interface, and (*ii*) in an acetone solution in water containing a ventilated gas bubble. The flows were visualized by tracer particles in the liquid and were recorded by a video camera. The experiment with the planar interface failed to show any Marangoni instability (probably due to the unwanted presence of some organic surface-active pollutants), but all experiments involving a curved interface showed clearly more or less vigorous Marangoni convection flows.

Dijkstra and Lichtenbelt [1] have presented evidence to support the view that at least some of the observed flows originated from so-called "macroscale" convective effects, that is, some flows were driven by macroscopic surface-tension gradients being initially present in the system. On the other hand, several flow patterns have been observed that can only be explained as being the result of "microscale" Marangoni instability. This type of instability leads to convective flow development because of the growing in time of infinitesimally small disturbances of some given initial state of the system.

In this paper, we investigate the influence of interface curvature on the onset of microscale Marangoni convection by analysing a simple heat-transfer system within the framework of linear stability theory. Neglecting gravity, we consider an infinitely long cylindrical annulus of liquid, either being heated from the outer (solid) boundary and having a gas–liquid interface on the inside ("interior" case), or being heated from the inner (solid) boundary and having an outside gas–liquid interface ("exterior" case). By use of a standard normal-mode analysis we determine the critical

Marangoni number for neutral stability of the unperturbed steady state in which flow velocity and pressure gradient are zero and temperature is a function of the radial coordinate only. In Section 2 the mathematical formulation of the problem is derived in dimensionless and linearized form and Section 3 presents the linear stability analysis, leading to the eigenvalue problems to be solved for the various types of one- and two-dimensional modes. In Section 4 we give numerical results for the critical Marangoni number for a number of values of the curvature parameter. These results are discussed in Section 5, and some concluding remarks are made in Section 6.

Finally we note that only a slight modification of the analysis is needed to cover the mass-transport case of a liquid layer containing a solute that can evaporate at the gas–liquid interface.

2. Mathematical formulation

Under zero-gravity conditions, an annular liquid layer of depth H is confined between two infinitely-long coaxial circular-cylinder surfaces, one of which (with radius a) is the gas–liquid interface, the other being a solid surface from which heat is transferred to the fluid. Two configurations will be distinguished: the *interior* case (case I) in which the solid surface has radius $a + H$, and the *exterior* case (case E) where it has radius $a - H$ ($a > H$), see Figs. 1a, b. So, the radius of curvature of the interface is equal to a in both cases, however, the sign of the curvature is differing. In both cases the geometry tends, in limit $a \to \infty$, to the *plane* case (case P) considered by Pearson [5].

Cylindrical polar coordinates (r, θ, z) and corresponding flow-velocity components (u, v, w) are defined as indicated in Fig. 1c; the time variable will be denoted by t, the pressure by p and the liquid temperature by $\mathscr{T}$. The liquid is taken to be homogeneous, incompressible and Newtonian with temperature-independent density ϱ, dynamic viscosity μ and heat-diffusion coefficient D. In the sequel it will be assumed that the gas–liquid interface always coincides with the cylinder surface $r = a$, even in presence of liquid motion.

The complete set of governing equations for u, v, w, p and $\mathscr{T}$ reads as follows (see Landau and Lifshitz [2]):

Momentum equations (Navier–Stokes equations):

$$u_t + uu_r + \frac{v}{r}u_\theta + wu_z - \frac{v^2}{r} = -\frac{1}{\varrho}p_r + \nu\left(\nabla^2 u - \frac{2}{r^2}v_\theta - \frac{u}{r^2}\right), \tag{2.1}$$

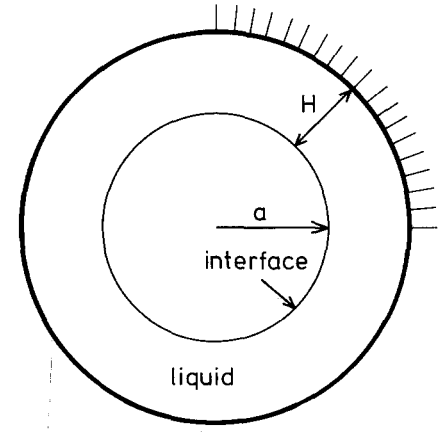

(a) INTERIOR

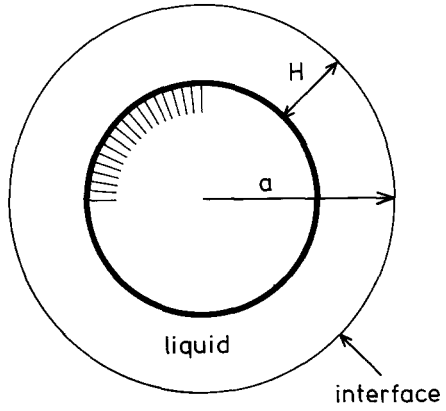

(b) EXTERIOR

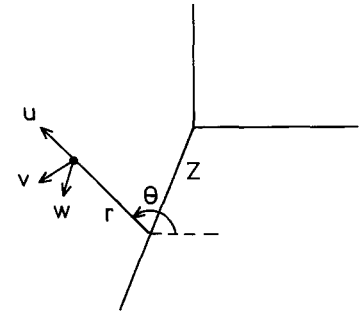

(c)

Fig. 1. (a) The interior case. (b) The exterior case. (c) Definition sketch.

$$v_t + uv_r + \frac{v}{r} v_\theta + wv_z + \frac{uv}{r} = -\frac{1}{\varrho r} p_\theta + \nu \left(\nabla^2 v + \frac{2}{r^2} u_\theta - \frac{v}{r^2} \right), \tag{2.2}$$

$$w_t + uw_r + \frac{v}{r} w_\theta + ww_z = -\frac{1}{\varrho} p_z + \nu \nabla^2 w, \tag{2.3}$$

where $\nu = \mu/\varrho$, $\nabla^2 = \partial^2/\partial r^2 + (1/r)\partial/\partial r + (1/r^2)\partial^2/\partial\theta^2 + \partial^2/\partial z^2$, and indices indicate partial differentiation;

Continuity equation:

$$u_r + \frac{1}{r} v_\theta + w_z + \frac{u}{r} = 0; \tag{2.4}$$

Heat-conduction equation with convection terms:

$$\mathscr{T}_t + u\mathscr{T}_r + \frac{v}{r} \mathscr{T}_\theta + w\mathscr{T}_z = D\nabla^2 \mathscr{T}. \tag{2.5}$$

The liquid is heated from the solid surface by keeping this surface at the constant temperature T_w. This gives the following boundary condition for the fluid temperature:

$$\mathscr{T} = T_w \quad \text{at the solid surface.} \tag{2.6}$$

The environment, that is, the region $0 \leqslant r < a$, $|z| < \infty$, in case I and $r > a$, $|z| < \infty$ in case E, is assumed to have a constant temperature $T_e < T_w$. At the interface we impose the boundary condition

$$\frac{\partial \mathscr{T}}{\partial r} = (+/-)\, \Lambda(\mathscr{T} - T_e) \quad \text{at } r = a \quad \text{(for case I/E)}, \tag{2.7}$$

where the sign difference arises from the different orientation of the radial coordinate r with respect to the liquid layer in the two cases. The positive constant Λ is an important physical parameter determining the rate of heat transfer from the liquid to the environment. Small values of Λ correspond to an "almost-insulating" interface, large values to a "well-conducting" one.

The unperturbed steady state, the stability of which will be studied in this paper, is characterized by zero flow velocity, zero pressure gradient and a

temperature distribution T_s depending only on r. The form of $T_s(r)$ is easily obtained from the steady-state heat-conduction equation without convection terms:

$$\frac{d^2T_s}{dr^2} + \frac{1}{r}\frac{dT_s}{dr} = 0.$$

The general solution of this equation can be written as

$$T_s(r) = (T_w - T_e)\{A \ln (r/H) + B\}, \tag{2.8}$$

where A and B denote dimensionless integration constants to be determined from boundary conditions (2.6) and (2.7) for $\mathscr{T}$ that, of course, also should be satisfied by T_s. Only A will be needed hereafter:

$$A = \begin{cases} \left[\frac{1}{a\Lambda} + \ln\left(\frac{a+H}{a}\right)\right]^{-1}, \text{ case I.} & \text{(2.9a)} \\ \left[-\frac{1}{a\Lambda} + \ln\left(\frac{a-H}{a}\right)\right]^{-1}, \text{ case E.} & \text{(2.9b)} \end{cases}$$

The governing equations (2.1)–(2.5) are now linearized about the unperturbed steady state by assuming that the flow velocity, the pressure gradient and the perturbation temperature $T = \mathscr{T} - T_s$ are infinitesimally small quantities. Using (2.8) for T_s, we get respectively:

$$u_t = -\frac{1}{\varrho}p_r + \nu\left(\nabla^2 u - \frac{2}{r^2}v_\theta - \frac{u}{r^2}\right), \tag{2.10}$$

$$v_t = -\frac{1}{\varrho r}p_\theta + \nu\left(\nabla^2 v + \frac{2}{r^2}u_\theta - \frac{v}{r^2}\right), \tag{2.11}$$

$$w_t = -\frac{1}{\varrho}p_z + \nu\nabla^2 w, \tag{2.12}$$

$$u_r + \frac{1}{r}v_\theta + w_z + \frac{u}{r} = 0, \tag{2.13}$$

$$T_t + \frac{u}{r}A(T_w - T_e) = D\nabla^2 T. \tag{2.14}$$

In terms of T, boundary conditions (2.6) and (2.7) read

$$T = 0 \quad \text{at the solid surface,} \tag{2.15}$$

$$T_r = (+/-)\,\Lambda T \quad \text{at } r = a \text{ (for case I/E).} \tag{2.16}$$

Further we have the no-slip condition

$$u = v = w = 0 \quad \text{at the solid surface.} \tag{2.17}$$

As stated earlier, the gas–liquid interface is assumed to remain at the location $r = a$, hence the radial velocity should vanish there:

$$u = 0 \quad \text{at} \quad r = a. \tag{2.18}$$

The surface tension, γ, enters the problem via the tangential-stress balance at the interface, its effect on the normal-stress balance being neglected. Assuming that the environment does not exert shear forces on the liquid at the interface, the θ- and z-component of the tangential-stress balance are respectively,

$$\frac{1}{r}\frac{\partial \gamma}{\partial \theta} = \tau_{(\theta)}, \quad \frac{\partial \gamma}{\partial z} = \tau_{(z)}, \tag{2.19}$$

where the right-hand sides denote the corresponding components of the shear stress at $r = a$. The stress components $\tau_{(\theta)}$ and $\tau_{(z)}$ can be expressed in terms of u, v and w (see Landau and Lifshitz [2]):

$$\left.\begin{aligned} \tau_{(\theta)} &= (-/+)\,\mu\left(v_r + \frac{1}{r}u_\theta - \frac{v}{r}\right) \\ \tau_{(z)} &= (-/+)\,\mu(u_z + w_r) \end{aligned}\right\} \quad \text{at } r = a \quad \text{(for case I/E).} \tag{2.20}$$

These expressions can be simplified by noting that $u_\theta = u_z = 0$ at $r = a$ by virtue of (2.18). The surface tension is taken to be the only physical property of the fluid that is temperature-dependent, $\gamma = \gamma(\mathscr{T})$, with $\gamma'(\mathscr{T}) < 0$. We shall assume that $\gamma'(\mathscr{T})$ is a (negative) constant in the temperature range under consideration. Using (2.20), boundary condition (2.19) can now be

written as

$$\left.\begin{aligned} \frac{1}{r}\gamma'(\mathscr{T})\,T_0 &= (-/+)\mu\left(v_r - \frac{v}{r}\right) \\ \gamma'(\mathscr{T})\,T_z &= (-/+)\mu w_r \end{aligned}\right\} \quad \text{at } r = a \quad \text{(for case I/E).} \tag{2.21}$$

The final step in the formulation of the boundary-value problem is the introduction of the dimensionless quantities (indicated by asterisks)

$$(r^*, z^*) = (r, z)/H, \quad t^* = V_{\text{ref}}\, t/H, \quad T^* = T/(T_w - T_e),$$

$$(u^*, v^*, w^*) = (u, v, w)/V_{\text{ref}}, \quad p^* = p/(\varrho V_{\text{ref}}^2),$$

where V_{ref} denotes some reference velocity. After dropping the asterisks, the non-dimensional form of the linearized boundary-value problem (2.10)–(2.18), (2.21) reads as follows:

Differential equations

$$u_t = -p_r + \frac{1}{\text{Re}}\left(u_{rr} + \frac{1}{r^2}u_{00} + u_{zz} + \frac{1}{r}u_r - \frac{2}{r^2}v_0 - \frac{u}{r^2}\right), \tag{2.22}$$

$$v_t = -\frac{1}{r}p_0 + \frac{1}{\text{Re}}\left(v_{rr} + \frac{1}{r^2}v_{00} + v_{zz} + \frac{1}{r}v_r + \frac{2}{r^2}u_0 - \frac{v}{r^2}\right), \tag{2.23}$$

$$w_t = -p_z + \frac{1}{\text{Re}}\left(w_{rr} + \frac{1}{r^2}w_{00} + w_{zz} + \frac{1}{r}w_r\right), \tag{2.24}$$

$$u_r + \frac{1}{r}v_0 + w_z + \frac{u}{r} = 0, \tag{2.25}$$

$$T_t + A\frac{u}{r} = \frac{1}{\text{Pe}}\left(T_{rr} + \frac{1}{r^2}T_{00} + T_{zz} + \frac{1}{r}T_r\right); \tag{2.26}$$

Boundary conditions
at the solid surface $r = a/H + 1$ (case I), or $r = a/H - 1$ (case E):

$$u = v = w = T = 0; \tag{2.27}$$

at the interface $r = a/H$:

$$\left.\begin{aligned} u &= 0, && (2.28)\\ T_r &= (+/-)LT && (2.29)\\ \frac{\mathrm{Ma}}{r} T_0 &= (+/-)\,\mathrm{Pe}\left(v_r - \frac{v}{r}\right) && (2.30)\\ \mathrm{Ma}\, T_z &= (+/-)\,\mathrm{Pe}\, w_r && (2.31) \end{aligned}\right\} \quad \text{(for case I/E).}$$

The following dimensionless numbers have been introduced here:

$$\mathrm{Re} = \frac{HV_{\mathrm{ref}}}{\nu} \quad \text{(Reynolds number)},$$

$$\mathrm{Pe} = \frac{HV_{\mathrm{ref}}}{D} \quad \text{(Péclet number)},$$

$$L = H\Lambda \quad \text{(coefficient of heat-transfer at the interface)},$$

$$\mathrm{Ma} = -(T_{\mathrm{w}} - T_{\mathrm{e}})\gamma'(\mathscr{T})\frac{H}{\mu D} \quad \text{(Marangoni number)}.$$

and A is given by (2.9).

We conclude this section with some remarks.

1. For systems with $\gamma'(\mathscr{T}) > 0$, one should necessarily have $T_{\mathrm{e}} > T_{\mathrm{w}}$ for Marangoni instability to occur; the analysis remains essentially unchanged.
2. If μ, ρ and D are temperature-dependent, the analysis of this paper is still feasible. However, it will become more complicated, because T_{s} then satisfies a nonlinear equation and additional r-dependent coefficients (determined by T_{s}) will appear in the linearized boundary-value problem.
3. In the plane case, Pearson's Marangoni number B is equal to $L(L + 1)^{-1}$ Ma, so B is dependent on L.

3. Stability analysis

Small disturbances of the unperturbed state should satisfy boundary-value problem (2.22)–(2.31). We are interested in determining the circumstances

under which a small disturbance will have a tendency to diminish in time (stability) or to grow in time (instability). The latter possibility can be seen as the initial stage of roll-cell formation in the liquid. However, for a complete description of the evolution of the flow from an initially small disturbance into a complete roll-cell pattern the present linearized model is clearly inadequate.

Mathematically speaking, we wish to study the stability of the trivial solution $u = v = w = p = T = 0$ of boundary-value problem (2.22)–(2.31). A standard approach for linear problems is a normal-mode analysis, in which it is argued that the behaviour of an arbitrary disturbance can be studied by looking at the Fourier components (normal modes or normal waves) into which it can be decomposed:

$$\{u, v, w, p, T\}(r, \theta, z, t) = \{U(r), V(r), W(r), \mathrm{Re}^{-1}P(r), \mathrm{iPe}\,\Theta(r)\}\mathrm{e}^{in\theta}\mathrm{e}^{i\alpha z}\mathrm{e}^{\beta t}. \tag{3.1}$$

In fact this is a separation-of-variables technique which reduces the problem to solving a set of *ordinary* differential equations for U, V, W, P and Θ. The integer n is the azimuthal wave-number, α denotes the axial wave number, and β is a (possibly complex) constant which determines the growth or decay in time of the mode. The case $\mathscr{R}e(\beta) > 0$ corresponds to instability, $\mathscr{R}e(\beta) < 0$ means stability, and $\mathscr{R}e(\beta) = 0$ will be referred to as neutral (or marginal) stability.

Using (3.1), problem (2.22)–(2.31) becomes

$$\mathrm{Re}\,\beta\, U = -P' + U'' - \frac{n^2}{r^2}U - \alpha^2 U + \frac{1}{r}U' - \frac{2in}{r^2}V - \frac{1}{r^2}U, \tag{3.2}$$

$$\mathrm{Re}\,\beta\, V = -\frac{in}{r}P + V'' - \frac{n^2}{r^2}V - \alpha^2 V + \frac{1}{r}V' + \frac{2in}{r^2}U - \frac{1}{r^2}V, \tag{3.3}$$

$$\mathrm{Re}\,\beta\, W = -i\alpha P + W'' - \frac{n^2}{r^2}W - \alpha^2 W + \frac{1}{r}W', \tag{3.4}$$

$$U' + \frac{in}{r}V + i\alpha W + \frac{1}{r}U = 0, \tag{3.5}$$

$$\mathrm{Pe}\,\beta\,\Theta - \frac{iA}{r}U = \Theta'' - \frac{n^2}{r^2}\Theta - \alpha^2\Theta + \frac{1}{r}\Theta', \tag{3.6}$$

subject to the boundary conditions

$$U = V = W = \Theta = 0 \quad \text{at} \begin{cases} r = \dfrac{a}{H} + 1 & \text{(case I)}, \\ r = \dfrac{a}{H} - 1 & \text{(case E)}, \end{cases} \tag{3.7}$$

$$\left.\begin{aligned} U &= 0 && (3.8) \\ \Theta' &= (+/-)L\Theta && (3.9) \\ \frac{n}{r}\,\mathrm{Ma}\,\Theta &= (-/+)\left(V' - \frac{V}{r}\right) && (3.10) \\ \alpha\,\mathrm{Ma}\,\Theta &= (-/+)W' && (3.11) \end{aligned}\right\} \quad \text{at } r = \frac{a}{H} \quad \text{for case I/E,}$$

where the primes denote differentiation with respect to r. This boundary-value problem can be viewed as an eigenvalue problem from which, for given values of the parameters Ma, Pe, Re, L, a/H, the behaviour as $t \to \infty$ of a particular mode with wave-number pair (n, α) is determined by the corresponding value of the eigenvalue β. This problem will be addressed in a future paper.

The present study, however, is concerned with the somewhat easier problem of determining the values of the Marangoni number Ma for which neutral stability occurs. We shall assume that the so-called "principle of exchange of stability" holds, that is, if $\mathscr{R}e(\beta) = 0$ then automatically $\mathscr{I}m(\beta) = 0$. The neutral state is then stationary rather than oscillatory ($\mathscr{I}m(\beta) \neq 0$). For certain systems, in which instability is solely caused by surface-tension effects, the principle has been proved by Vidal and Acrivos [7]. The cases for which it is known that oscillatory neutral states occur, always have two competing instability mechanisms. Therefore, in our analysis, β is put equal to zero and Ma is considered as the eigenvalue that has to be determined as a function of the wave-number pair (n, α) for a fixed pair of values of the remaining parameters L and a/H. Note that the dependence on Re and Pe has now dropped out of the problem. The minimum value of Ma is called the critical Marangoni number ($\mathrm{Ma}_{\mathrm{crit}}$), the corresponding wave-number pair $(n, \alpha)_{\mathrm{crit}}$ belonging to the so-called critical normal wave. Hence, the unperturbed state of the physical system is stable for $\mathrm{Ma} < \mathrm{Ma}_{\mathrm{crit}}$, and it will be unstable for $\mathrm{Ma} > \mathrm{Ma}_{\mathrm{crit}}$, the critical normal-wave component of any disturbance amplifying first for Ma-values exceeding $\mathrm{Ma}_{\mathrm{crit}}$ only slightly.

In the subsequent analysis we shall consider the two types of one-dimensional modes: (*i*) *azimuthal* waves (z-independent, $W = 0$, wave-number pair $(n, 0)$), and (*ii*) *axial* waves (θ-independent, $V = 0$, wave-number pair $(0, \alpha)$), separately from the remaining two-dimensional modes: (*iii*) *mixed modes* ($n > 0$, $\alpha > 0$).

(*i*) *Azimuthal waves*

For azimuthal waves we have $W = 0$ and further u, v, p and T do not depend on z, so the axial wave number α is equal to zero. The ultimate roll-cell pattern which might be imagined to develop from this type of disturbances consists of a number of cells of cylindrical shape (with generators parallel to the z-axis) arranged in a regular fashion over the annular cross-section of the fluid layer.

By introduction of a "stream function" $\Psi(r)$ with

$$U = \frac{in}{r}\Psi, \quad V = -\Psi', \tag{3.12}$$

continuity equation (3.5) is satisfied automatically. Next, after putting $\beta = 0$ and eliminating P from (3.2) and (3.3), we obtain two Cauchy-type equations involving Ψ and Θ:

$$\Psi^{iv} + \frac{2}{r}\Psi^{iii} - \frac{1 + 2n^2}{r^2}\Psi'' + \frac{1 + 2n^2}{r^3}\Psi' + \frac{n^4 - 4n^2}{r^4}\Psi = 0, \tag{3.13}$$

$$\Theta'' + \frac{1}{r}\Theta' - \frac{n^2}{r^2}\Theta = \frac{nA}{r^2}\Psi, \tag{3.14}$$

with boundary conditions

$$\Psi = \Psi' = \Theta = 0 \quad \text{at} \quad \begin{cases} r = \dfrac{a}{H} + 1 & \text{(case I)}, \\ r = \dfrac{a}{H} - 1 & \text{(case E)}, \end{cases} \tag{3.15}$$

$$\left.\begin{aligned} &\Psi = 0 && (3.16) \\ &\Theta' = (+/-)L\Theta && (3.17) \\ &n\mathrm{Ma}\,\Theta = (+/-)(r\Psi'' - \Psi') && (3.18) \end{aligned}\right\} \quad \text{at } r = \frac{a}{H} \quad \text{(for case I/E)}.$$

A straightfoward calculation shows that the general solution of (3.13) and (3.14) can be expressed in terms of the functions $r^{\pm n}$, $r^{2\pm n}$, $r^{\pm n} \ln(r)$ in the case $n \neq 1$, and $r^{\pm 1}$, $r^{\pm 1} \ln(r)$, r^3, $r \ln^2(r)$ in the case $n = 1$, involving six integration constants. Substitution into the boundary conditions (3.15)–(3.18) yields a set of six homogeneous linear algebraic equations for these constants. Upon equating to zero the coefficient determinant of this set a *linear* equation is obtained for the eigenvalue Ma, from which Ma follows as a function of n, L and a/H. We omit further details since the Ma-values have been computed numerically (see Section 4), and the above analytical approach has been used only to check the numerical results.

(*ii*) *Axial waves*

In the axially symmetric case we put $V = 0$ and $n = 0$. The corresponding roll-cells that might develop in this case will have toroidal shape, analogous to the toroidal eddies observed in axisymmetric Couette flow between concentric cylinders (Townsend [6]).

Continuity equation (3.5) is satisfied by putting

$$U = -\mathrm{i}\alpha\Phi, \quad W = \Phi' + \frac{1}{r}\Phi. \tag{3.19}$$

The equation for the "stream function" Φ is obtained after putting $\beta = 0$ and eliminating P from (3.2) and (3.4):

$$(\mathfrak{D} - \alpha^2)^2\Phi = 0, \quad \mathfrak{D} = \frac{\mathrm{d}^2}{\mathrm{d}r^2} + \frac{1}{r}\frac{\mathrm{d}}{\mathrm{d}r} - \frac{1}{r^2}. \tag{3.20}$$

The equation for Θ becomes

$$\Theta'' + \frac{1}{r}\Theta' - \alpha^2\Theta = -\frac{\alpha A}{r}\Phi. \tag{3.21}$$

The boundary conditions for (3.20) and (3.21) are

$$\Phi = \Phi' = \Theta = 0 \quad \text{at} \quad \begin{cases} r = \dfrac{a}{H} + 1 & \text{(case I)}, \\ r = \dfrac{a}{H} - 1 & \text{(case E)}, \end{cases} \tag{3.22}$$

$$\left.\begin{aligned} \Phi &= 0 && (3.23)\\ \Theta' &= (+/-)L\Theta && (3.24)\\ \alpha \mathrm{Ma}\Theta &= (-/+)\mathfrak{D}\Phi && (3.25) \end{aligned}\right\} \quad \text{at } r = \frac{a}{H} \quad \text{(for case I/E).}$$

As in the preceding case of azimuthal waves the details of the general solution of (3.20) and (3.21) can be pursued quite far analytically. Finally, this leads again to a linear equation for the eigenvalue Ma containing complicated expressions involving single and double integrals over products of modified Bessel functions (of order zero and one) and their derivatives. This approach has only been used in order to check the numerical results for this case.

(iii) Mixed modes

In this case we have both $n > 0$ and $\alpha > 0$. To satisfy continuity equation (3.5) we introduce two "stream functions", Φ and Ψ, by putting

$$U = \frac{in}{r}\Psi - i\alpha\Phi, \tag{3.26}$$

$$V = -\Psi', \tag{3.27}$$

$$W = \Phi' + \frac{1}{r}\Phi. \tag{3.28}$$

This transformation is just a simple linear combination of the ones we used for cases *(i)* and *(ii)*.

Now we put $\beta = 0$ in (3.2)–(3.4) and (3.6), and we eliminate P, first from (3.2) and (3.3), and next from (3.3) and (3.4). This leads to an 8th-order system of equations for U, V, W and Θ. After substitution of (3.26)–(3.28) we obtain the following 9th-order system of equations for Φ, Ψ and Θ:

$$\Psi^{iv} + \frac{2}{r}\Psi^{iii} - \left(\frac{1 + 2n^2}{r^2} + \alpha^2\right)\Psi'' + \left(\frac{1 + 2n^2}{r^3} - \frac{\alpha^2}{r}\right)\Psi'$$

$$+ \left(\frac{n^2 - 4n^2}{r^4} + \frac{\alpha^2 n^2}{r^2}\right)\Psi + \frac{n\alpha}{r}\left[\Phi'' - \frac{1}{r}\Phi' - \left(\frac{n^2}{r^2} + \alpha^2 - \frac{1}{r^2}\right)\Phi\right] = 0, \tag{3.29}$$

$$\Phi^{iii} + \frac{2}{r}\Phi'' - \left(\frac{n^2}{r^2} + \alpha^2 + \frac{1}{r^2}\right)\Phi' + \left(-\frac{n^2}{r^3} - \frac{3\alpha^2}{r} + \frac{1}{r^3}\right)\Phi$$

$$+ \frac{\alpha r}{n}\left[\Psi^{iii} + \frac{1}{r}\Psi'' - \left(\alpha^2 + \frac{n^2}{r^2} + \frac{1}{r^2}\right)\Psi' + \frac{2n^2}{r^3}\Psi\right] = 0, \quad (3.30)$$

$$\Theta'' + \frac{1}{r}\Theta' - \frac{n^2}{r^2}\Theta - \alpha^2\Theta = \frac{nA}{r^2}\Psi - \frac{A\alpha}{r}\Phi. \quad (3.31)$$

The increase of order of the system gives us the freedom to add a boundary condition, an obvious and very convenient choice being to normalize Ψ to zero on the solid surface. Then we have the following 9 boundary conditions to complete the eigenvalue problem for the mixed modes:

$$\Psi = \Psi' = \Phi = \Phi' = \Theta = 0 \text{ at } \begin{cases} r = \dfrac{a}{H} + 1 & \text{(case I)}, \\ r = \dfrac{a}{H} - 1 & \text{(case E)}, \end{cases} \quad (3.32)$$

$$\left.\begin{aligned} &\frac{n}{r}\Psi - \alpha\Phi = 0 && (3.33)\\ &\Theta' = (+/-)L\Theta && (3.34)\\ &\mathrm{Ma}\,\Theta = (+/-)(r\Psi'' - \Psi')/n && (3.35)\\ &\mathrm{Ma}\,\Theta = (-/+)\left(\Phi'' + \frac{1}{r}\Phi' - \frac{1}{r^2}\Phi\right)/\alpha && (3.36) \end{aligned}\right\} \text{ at } r = \frac{a}{H} \text{ (for case I/E).}$$

4. Numerical results

For each of the cases (*i*)–(*iii*) the corresponding eigenvalue problem has been solved numerically by a simple shooting technique. In the mixed-mode case (*iii*), the solution of (3.29) and (3.30) satisfying the first four boundary conditions of (3.32) can be written as a linear combination of three linearly independent solutions $(\Psi, \Phi)_i$, $i = 1, 2, 3$:

$$(\Psi, \Phi) = C_1(\Psi, \Phi)_1 + C_2(\Psi, \Phi)_2 + C_3(\Psi, \Phi)_3 \quad (4.1)$$

where the basic solutions $(\Psi, \Phi)_i$, $i = 1, 2, 3$, satisfy the initial conditions $(\Psi, \Psi', \Psi'', \Psi^{iii}, \Phi, \Phi', \Phi'') = (0, 0, 1, 0, 0, 0, 0)$, $(0, 0, 0, 1, 0, 0, 0)$ or $(0, 0, 0, 0, 0, 0, 1)$, respectively, at the solid surface. In a similar manner the solution of the temperature equation (3.31) satisfying the last of boundary conditions (3.32) can be written in terms of three particular solutions, $C_1\Theta_1$, $C_2\Theta_2$ and $C_3\Theta_3$, and one homogeneous solution, Θ_4,

$$\Theta = C_1\Theta_1 + C_2\Theta_2 + C_3\Theta_3 + C_4\Theta_4, \tag{4.2}$$

all four basic solutions Θ_i, $i = 1, \ldots, 4$, satisfying the initial condition $(\Theta, \Theta') = (0, 1)$ at the solid surface. The seven basic solutions involved in (4.1) and (4.2) have been computed by a 4th-order Runge–Kutta method.

Substitution of (4.1) and (4.2) in the remaining four boundary conditions (3.33)–(3.36) at the interface leads to a set of four homogeneous linear algebraic equations for the integration constants $C_1, \ldots, C_4$. Equating to zero the coefficient determinant we obtain the eigenvalue equation for Ma which has the following global structure:

$$\begin{vmatrix} a_{11} & a_{12} & a_{13} & 0 \\ a_{21} & a_{22} & a_{23} & a_{24} \\ b_1\mathrm{Ma} + a_{31} & b_2\mathrm{Ma} + a_{32} & b_3\mathrm{Ma} + a_{33} & b_4\mathrm{Ma} + a_{34} \\ b_1\mathrm{Ma} + a_{41} & b_2\mathrm{Ma} + a_{42} & b_3\mathrm{Ma} + a_{43} & b_4\mathrm{Ma} + a_{44} \end{vmatrix} = 0.$$

where the a_{ij}'s and the b_i's are independent of Ma. After evaluation of the determinant this yields a linear equation for Ma from which Ma follows as a function of the parameters n, α, L and a/H.

In the lower-dimensional cases (*i*) and (*ii*) the shooting method involves only five basic solutions to be computed numerically and three integration constants. The 3×3 coefficient determinant also leads to a linear equation for Ma.

In Table 1 and Fig. 2 we have collected numerical results for both the interior case (I) and exterior case (E) for two values of L, viz. $L = 1$ and $L = 12$, the first being a typical "small" value of L representing a badly-conducting gas–liquid interface and the latter being a typical "large" value of L representative of a well-conducting interface. For a range of values of the curvature parameter a/H, critical Marangoni numbers Ma_{crit} and corresponding wave-number pairs $(n, \alpha)_{crit}$ have been determined as follows. For each fixed pair $(L, a/H)$ the eigenvalues Ma have been computed for quite a large array of pairs (n, α) with $n = 0, 1, 2, \ldots$, and $\alpha = 0, 0.1, 0.2, \ldots$.

Table 1. Critical Marangoni numbers Ma_{crit} and corresponding critical wave-number pairs (n, α) for various values of the curvature parameter a/H for the interior case (I) and the exterior case (E). Results have been given for $L = 1$ (badly-conducting interface) and for $L = 12$ (well-conducting interface). The value $a/H = \infty$ refers to the plane case (P) and α_P denotes the (single) critical wave number for that case

Interior case (I)

	$L = 1$		$L = 12$	
a/H	Ma_{crit}	Critical mode (n, α)	Ma_{crit}	Critical mode (n, α)
0.1	1041.4	(1, 1.41)	531.0	(1, 1.53)
0.2	581.4	(1, 1.60)	490.1	(1, 1.94)
0.3	456.3	(1, 1.86)	480.0	(2, 1.04)
0.4	396.6	(1, 2.02)	459.9	(2, 1.37)
0.5	361.1	(1, 2.12)	459.2	(2, 1.66)
0.6	337.6	(1, 2.17)	463.9	(2, 1.90)
0.7	321.0	(1, 2.21)	469.2	(2, 2.09)
0.8	308.7	(1, 2.23)	469.8	(3, 1.35)
0.9	299.1	(2, 1.78)	471.2	(3, 1.60)
1.0	291.6	(2, 1.86)	473.8	(3, 1.80)
2.0	259.3	(0, 2.32)	489.8	(5, 1.87)
4.0	244.8	(0, 2.29)	501.7	(9, 1.90)
6.0	240.4	(0, 2.27)	506.6	(13, 1.91)
8.0	238.3	(0, 2.27)	509.2	(17, 1.92)
10.0	237.0	(0, 2.26)	510.8	(19, 2.10)
10^2	232.7	(0, 2.25)	517.3	(100, 2.59)
10^3	232.3	(0, 2.25)	518.0	(1000, 2.59)
∞	232.254	$\alpha_P = 2.246$	517.980	$\alpha_P = 2.775$

Exterior case (E)

	$L = 1$		$L = 12$	
a/H	Ma_{crit}	Critical mode (n, α)	Ma_{crit}	Critical mode (n, α)
1.01	243.7	(1, 0.94)	1166.5	(1, 1.47)
1.1	188.3	(1, 1.10)	785.4	(1, 1.73)
1.2	193.0	(1, 1.32)	707.0	(2, 1.12)
1.3	187.5	(2, 0)	652.0	(2, 1.37)
1.4	187.1	(2, 0.57)	627.8	(2, 1.60)
1.5	189.9	(2, 0.92)	615.2	(2, 1.80)
1.6	194.0	(2, 1.15)	606.2	(3, 1.08)
1.7	195.0	(3, 0.01)	593.6	(3, 1.36)
1.8	195.3	(3, 0.05)	585.8	(3, 1.57)
1.9	197.5	(3, 0.66)	580.6	(3, 1.74)
2.0	200.0	(3, 0.94)	576.7	(3, 1.88)
4.0	214.9	(8, 0)	540.7	(8, 1.60)
6.0	220.8	(12, 0.50)	532.1	(13, 1.48)
8.0	223.5	(17, 0)	528.2	(19, 1.17)
10.0	225.3	(21, 0.38)	526.0	(25, 0.93)
10^2	231.6	(200, 1.00)	518.9	(200, 1.91)
10^3	232.2	(2000, 1.02)	518.2	(2000, 1.92)
∞	232.254	$\alpha_P = 2.246$	517.980	$\alpha_P = 2.775$

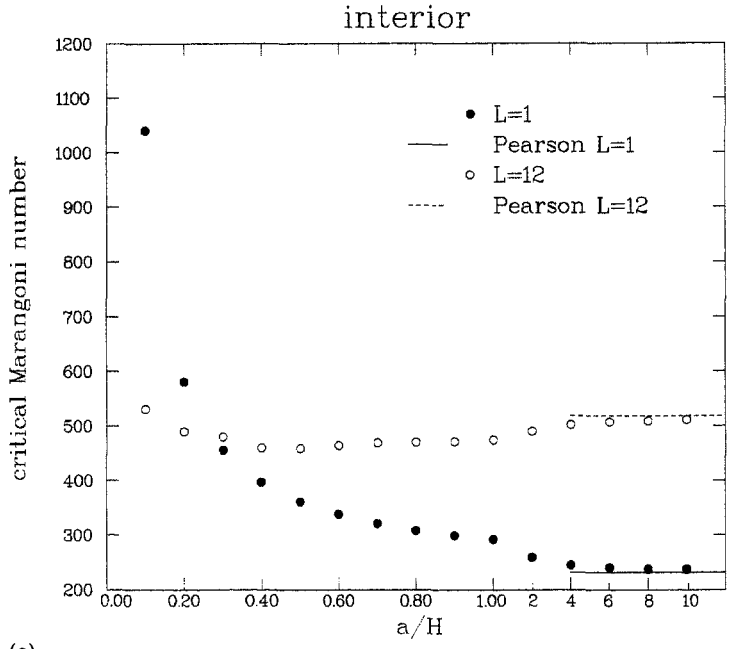

(a)

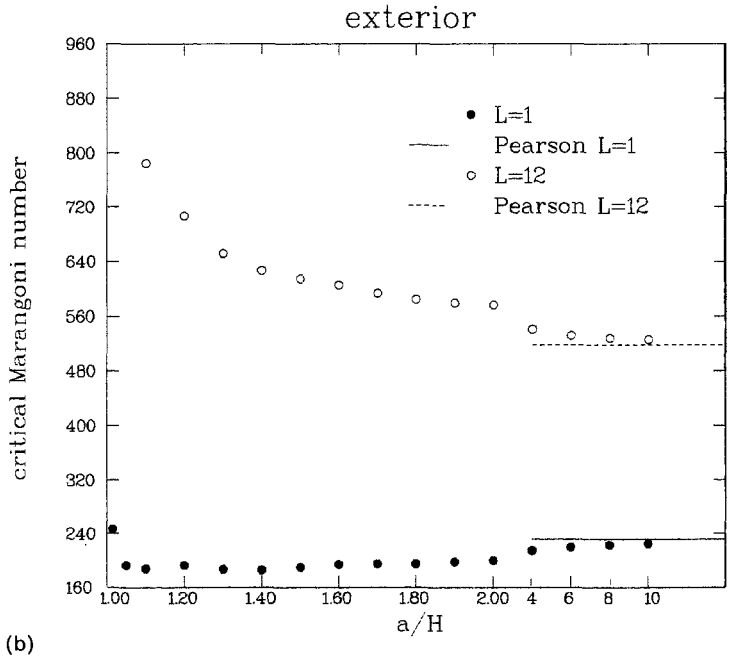

(b)

Fig. 2. Graphical representation of numerical results given in Table 1 for critical Marangoni number vs. curvature a/H. Note that the scale of the horizontal axes is not uniform.

From the resulting two-dimensional array of Ma-values a first estimate for Ma_{crit} and $(n, \alpha)_{crit}$ was obtained by inspection. Next the entries of Table 1 were determined by interpolation in the α-direction.

In the limit $a/H \to \infty$ our results should tend to those of Pearson [5] for the plane case (P) which have also been included in Table 1. This property is confirmed by the results for some large values of a/H (10^2 and 10^3). Note that for case P there is only a single wave number (α_P) so that one should have:

$$\lim_{a/H \to \infty} \left[\left(\frac{nH}{a} \right)^2 + \alpha^2 \right]^{1/2} = \alpha_P .$$

5. Discussion of results

The most striking aspect of our results as presented in Table 1 and Fig. 2 can be roughly described as follows. For a fixed value of a/H, we have for a badly-conducting interface (small L) that the interior case (I) is more stable than the plane case (P), whereas the exterior case (E) is less stable than case P. However, for a well-conducting interface (large L) the stability behaviour of cases I and E is just the other way round. In this statement we have ignored for the moment the behaviour of case I for large L and small a/H and of case E for small L and a/H close to 1. The results can be explained from a consideration of the physical mechanisms involved.

Case I: When compared with case P, case I has always a geometrical disadvantage with regard to the onset of Marangoni convection flows, since per unit of interface area case I possesses more stabilizing solid-surface area than case P. On the other hand, the steady heat flux (per unit area) through the interface, ϕ, is larger for case I than for case P. This puts case I in an advantageous position. However, for small L the interface is badly conducting and ϕ is small. Moreover, for small L, a local temperature rise at the interface will mainly vanish by conduction of heat into the liquid. Comparing cases I and P, the diffusion of heat will take place more rapidly in case I, because of the simple argument that in case I there is more liquid in the immmediate neighbourhood of the "hot spot" for the heat to diffuse into than in case P. Consequently, temperature differences along the interface will be smaller in case I and also the induced surface tractions. This disadvantage, combined with the geometrical disadvantage mentioned earlier, is likely to dominate the heat-flux advantage so that case I is more stable than case P when L is small. For very small values of a/H the steady temperature tends to the constant value T_w everywhere in the liquid, and this

Table 2. Critical Marangoni numbers for $L = 3.5, 3.6$ and $a/H = 1.5, 2, 2.5$ for interior case (I) and exterior case (E), showing transition of stability behaviour for $a/H = 2$

$L = 3.5$	$a/H = 1.5$	$a/H = 2$	$a/H = 2.5$
case I	264.4	262.0	260.8
case E	267.9	261.1	258.7
$L = 3.6$	$a/H = 1.5$	$a/H = 2$	$a/H = 2.5$
case I	266.4	264.2	263.1
case E	271.9	264.6	262.0

explains why $\mathrm{Ma}_{\mathrm{crit}} \to \infty$ for $a/H \downarrow 0$ in case I (not only for $L = 1$, but for all L).

When L is large, the interface is well-conducting so that temperature disturbances at the interface will decay rapidly and no significant differences will occur in the resulting surface tractions between cases I and P when they would be subjected to the same local temperature disturbances at the interface. On the other hand, the difference between ϕ for case I and for case P is now sufficiently large to dominate the geometrical disadvantage of case I and this makes case I less stable than case P, except for very small values of a/H, for which $\mathrm{Ma}_{\mathrm{crit}}$ tends to infinity again.

Case E: The stability behaviour of case E is just the opposite of that of case I. It can be explained in a similar way by noticing (*i*) that case E has a geometrical advantage over case P, (*ii*) that it has a smaller heat flux ϕ than case P, (*iii*) that (for small L) a local temperature rise at the interface will vanish more slowly by diffusion of heat into the liquid than in case P, and (*iv*) that for $a/H \downarrow 1$ the steady temperature tends to a constant value everywhere in the liquid, so that $\mathrm{Ma}_{\mathrm{crit}} \to \infty$.

Numerical tests show that the transition in stability behaviour occurs for L about 3.5. A more precise statement cannot be made since the transition value turns out to be weakly dependent on a/H. This is illustrated by Table 2 from which it can be seen that for $a/H = 2$ the transition takes place at a value of L between 3.5 and 3.6. On the other hand, Table 2 shows that for $a/H = 1.5$ the transition value is smaller than 3.5, while it is larger than 3.6 for $a/H = 2.5$.

6. Concluding remarks

From our results it can be concluded that curvature of the gas/liquid interface exerts a noticeable influence on the onset of microscale Marangoni instability. Whether it has a stabilizing or destabilizing effect depends on the measure of conductiveness of the interface and on the orientation (convex

or concave) and magnitude of the curvature. It is to be expected that the results will hold also, in a global sense, for curved interfaces of non-cylindrical shape. In a forthcoming paper similar behaviour is demonstrated for a liquid layer confined between two concentric spherical surfaces.

In practical situations, Marangoni numbers often turn out to be much larger than the critical ones following from our calculations. Disregarding for the moment the possible presence of macroscale Marangoni effects, this will mean that a liquid layer with an initially uniform temperature or concentration profile will become unstable before the steady situation (the stability of which we have studied here) will have been established. In this sense our critical Marangoni numbers could be considered as upper bounds for stability. In the experiments described in the Introduction typical values of Ma and L were 10^8 and 10, respectively. Indeed, the video recordings show that the onset of Marangoni convection flows takes place almost immediately after the creation of the gas–liquid interface. However, it has not been possible to collect quantitative data on critical Marangoni numbers from these experiments and, as far as we know, no other experimental data are available at this moment. Therefore, the experimental verification of our theoretical results will have to be postponed. Future experiments to test the theory are in preparation.

The better insight into the influence of the interface curvature on the onset of roll-cell activity offers the possibility of improving the design of industrial structured-packing materials. These are commonly composed of wavy metal plates along which liquid films flow. Our results might lead to the use of different packing materials depending on whether the heat- or mass-transfer takes place in a high-L or a low-L regime.

References

1. Dijkstra, H.A. and Lichtenbelt, J.H.: Mass transfer driven Marangoni convection under micro-gravity. *Appl. Microgravity Tech.* 1 (1988) 180–187.
2. Landau, L.D. and Lifshitz, E. M.: *Fluid Mechanics.* Pergamon Press (1959).
3. Lichtenbelt, J.H., Drinkenburg, A.A.H. and Dijkstra, H.A.: Marangoni convection and mass transfer from the liquid to the gas phase. *Naturwissenschaften* 73 (1986) 356–359.
4. Nield, D.A.: Surface tension and buoyancy effects in cellular convection. *J. Fluid Mech.* 19 (1964) 341–352.
5. Pearson, J.R.A.: On convection cells induced by surface tension. *J. Fluid Mech.* 4 (1958) 489–500.
6. Townsend, A.A.: Axisymmetric Couette flow at large Taylor numbers. *J. Fluid Mech.* 144 (1984) 329–362.
7. Vidal, A. and Acrivos, A.: Nature of the neutral state in surface tension driven convection. *Phys. Fluids* 9 (1966) 615–616.